Replacement of the heterologous 5′ untranslated region allows preservation of the fully functional activities of type 2 porcine reproductive and respiratory syndrome virus

Fei Gao [a], Huochun Yao [b], Jiaqi Lu [a], Zuzhang Wei [a], Haihong Zheng [a], Jinshan Zhuang [a], Guangzhi Tong [a,*], Shishan Yuan [a,*]

[a] Department of Swine Infectious Diseases, Shanghai Veterinary Research Institute, Chinese Academy of Agricultural Sciences, Shanghai 200241, PR China
[b] College of Veterinary Medicine, Nanjing Agricultural University, Nanjing, Jiangsu Province 210095, PR China

ARTICLE INFO

ABSTRACT

The 5′ untranslated region (UTR) is believed to be vital for the replication of porcine reproductive and respiratory syndrome virus (PRRSV), yet its functional mechanism remains largely unknown. In this study, to define the cis-acting elements for viral replication and infectivity, The 5′ UTR swapping chimeric clones pTLV8 and pSHSP5 were constructed based on two different genotypes full-length infectious cDNA clone pAPRRS and pSHE backbones. Between them, vTLV8 could be rescued from pTLV8 and had similar virological properties to vAPRRS, including phenotypic characteristic and RNA synthesis level. However, pSHSP5 exhibited no evidence of infectivity. Taken together, the results presented here demonstrate that only the 5′ UTR of type 1 PRRSV did not affect the infectivity and replication of type 2 PRRSV in vitro. The 5′ UTR of type 2 PRRSV could be functionally replaced by its counterpart from type 1.

© 2013 Elsevier Inc. All rights reserved.

Introduction

The 5′ untranslated region (UTR) of positive-sense, single-stranded RNA viruses has been demonstrated to play a key role in the regulation of viral replication and many biological properties. Research on many positive-sense RNA viruses has shown that their important secondary structure in the 5′ UTR protects against degradation by exonucleases (Gallie, 1998). For example, the 5′ cloverleaf plays a crucial role in maintaining the stability of poliovirus RNA (Barton et al., 2001) and a hairpin motif located close to the 5′ end is believed to be important for the stabilization of the RNA (TR and B, 1989). In Dengue virus, the 5′ UTR is also critical for RNA synthesis because a stem–loop RNA structure at the 5′ end promotes specific RNA synthesis (Alvarez et al., 2005; Lodeiro et al., 2009) and a binding site for viral RNA-dependent-RNA polymerase (RdRp) at the 5′ end of the genome facilitates template recognition at the 3′ end of the genome via long-range RNA–RNA interactions (Filomatori et al., 2007). The 5′ end of the Aichi virus genome encodes RNA elements important for both negative- strand and positive-strand RNA synthesis (Nagashima et al., 2005b). In addition to involvement in the stability of the

genome, the cloverleaf structure at the 5′ end of the poliovirus genome has been demonstrated to be essential for both plus- and minus-strand RNA synthesis (Andino et al., 1990; Gamarnik and Andino, 1998; Herold and Andino, 2000). Furthermore, in the case of alphaviruses, flaviviruses and some picornaviruses, the 5′ UTR has also been shown to contain distinct core promoter elements for RNA synthesis (Frolov et al., 2001; Frolov et al., 1998; Nagashima et al., 2005a). In addition, the 5′ UTR affects translational control. Internal ribosome entry site (Mihalek et al., 1999) function has been found in the 5′ UTR of some members of the Flaviviridae (Dumas et al., 2003) and Picornaviridae (Rijnbrand et al., 2000, 1997).

Porcine reproductive and respiratory syndrome (PRRS) emerged in the late 1990s in Europe and North America, resulting in tremendous economic loss to the swine industry. The PRRS viruses (PRRSV) isolated from Europe and North America display huge diversity in genetic and serological performance, although they induce indistinguishable clinical manifestations (Halbur et al., 1995; Nelsen et al., 1999). As a result, PRRSV has been characterized into two distinct genotypes, European type 1 and North American type 2 (Wang et al., 2008). PRRSV is a small, enveloped RNA virus, a member of the genus Arterivirus, family Arteriviridae, order Nidovirales (Cavanagh, 1997; Snijder, 2001). The PRRSV genome consists of at least ten open reading frames (ORFs), which are flanked by the 5′ and 3′ UTRs. The 5′ UTRs of the

type 1 and type 2 PRRSV are different in length (approximately 220 and 190 nucleotides (nt), respectively) and share approximately 60% nucleotide homology (Forsberg, 2005; Hanada et al., 2005; Lu et al., 2011). Nevertheless, highly conserved stem–loop structures have been identified in the leader of all PRRSV strains,

which are believed to play a part in viral replication (Oleksiewicz et al., 1999). PRRSV adopts a unique discontinuous transcription mechanism for sg mRNA transcription. The structural proteins are translated from the 5′ ends of a nested set of co-terminal sg (Khromykh et al., 2003) mRNA2 to 7 (Snijder and Meulenberg,
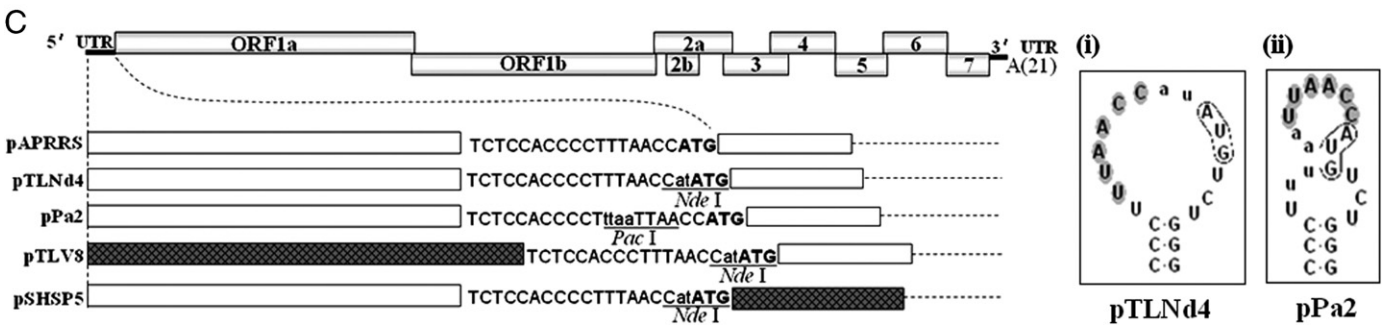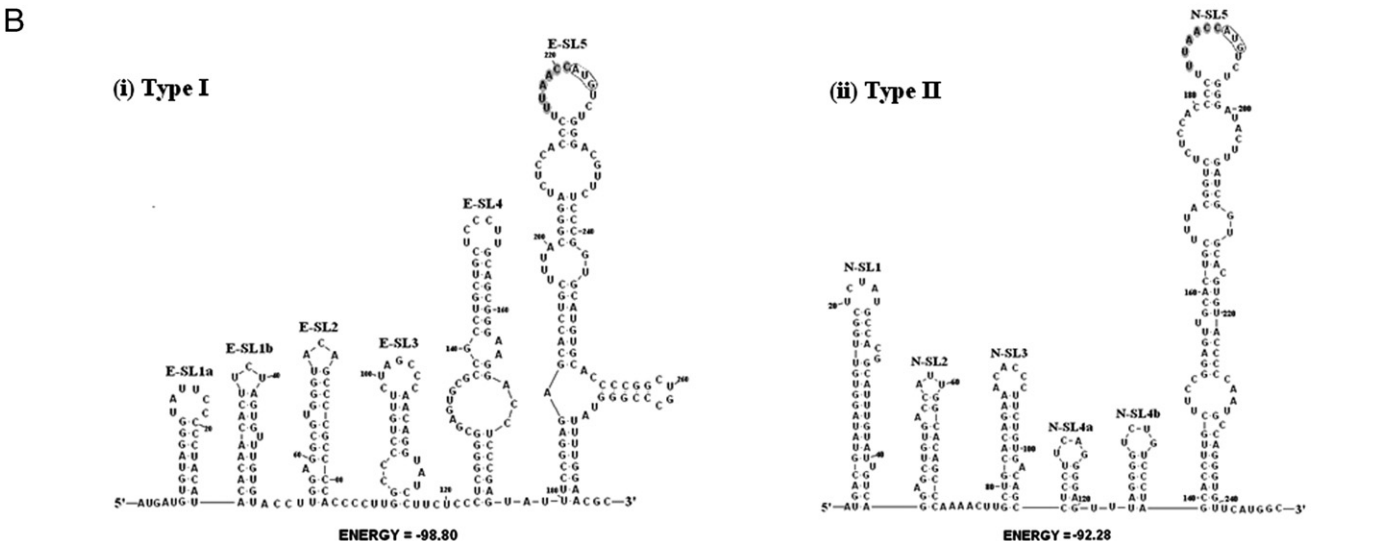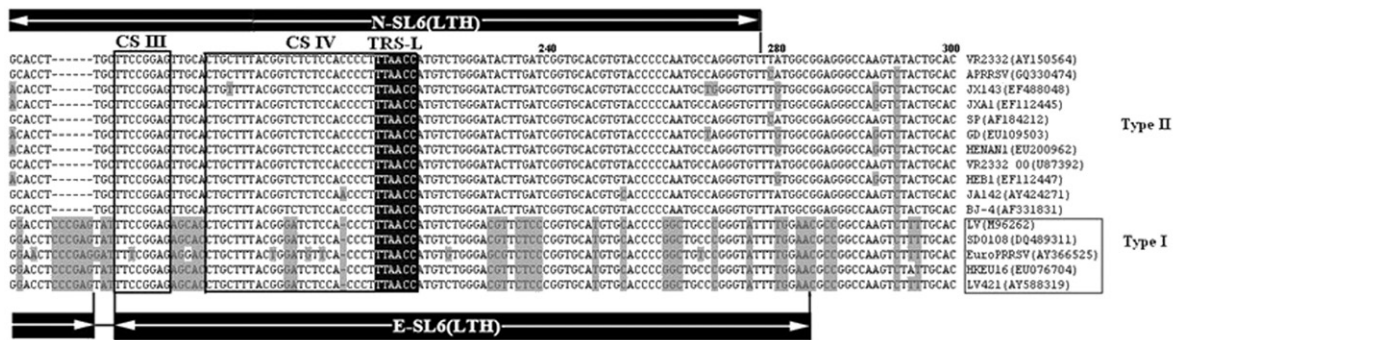
1998); (Alexander and Pasternak, 2006; Pasternak et al., 2006; Sawicki and Sawicki, 1995). With the exception of the smallest sg mRNA7, each sg mRNA is structurally polycistronic but functionally monocistronic because that only the 5′-proximal ORF is translated. However, sg mRNA2 is bicistronic and codes for ORFs 2a and 2b (Meulenberg et al., 1993b). The key elements that join the leader sequence to different segments (mRNA bodies) are the transcription-regulating sequence (TRS), which are essential for joining the leader to the body. For most coronaviruses and arteriviruses, the 5′ leader sequences are just the 5′-terminal portions of the 5′ UTR (Born et al., 2005), but PRRSV 5′ leader consists of its entire 5′ UTR.

The 5′ UTR of PRRSV is believed to be vital to the regulation of genomic RNA replication, transcription and mRNA translation, yet its function and regulatory mechanism remain largely unknown. In this study, we conducted inter-genotypic 5′ UTR swapping with the PRRSV infectious full-length cDNA clones pAPRRS and pSHE, in order to investigate the regulatory function of PRRSV 5′ UTR and the cis-acting elements in viral replication and infectivity. Our results demonstrated that replacement of the complete 5′ UTR of type 2 PRRSV by that of type 1 allowed all functions of the recipient virus to be maintained. However, 5′ UTR of type 1 could not be substituted with its counterpart of type 2. It could be accounted for the TRS-related stem–loop structure disruption. The resulting chimeric virus was genetically stable and displayed similar biologic characteristics to the parental virus, with respect to infectivity, growth curve and sg mRNA transcription in vitro. This is the first report that the nidovirus 5′ UTR can be replaced with that of a different genotype without functional alterations. Our findings suggest that high-ordered RNA structure plays an essential role in the replication of PRRSV. Thus, we can use this platform for future studies to define the basic biology of PRRSV.

Materials and methods

Cells and viruses

MARC-145 cells were grown in minimum essential medium (MEM) (Invitrogen) supplemented with 10% fetal bovine serum (FBS) (Gibco-BRL) and maintained in MEM with 2% FBS at 37 °C in a humidified 5% CO_2 atmosphere as described previously (Gao et al., 2012; Lu et al., 2011; Sun et al., 2010). Baby hamster kidney (BHK-21) cells were grown in Eagle's minimum essential medium (EMEM) (ATCC) supplemented with 10% FBS.

The type1 and type 2 PRRSV full-length infectious clones pSHE and pAPRRS were used in the present study as the backbones for 5′ UTR inter-genotypic substitution. vAPPRS (GenBank accession No. GQ330474; (Yuan and Wei, 2008) and vSHE (GenBank accession No. GQ461593; Yuan et al., unpublished data) were rescued from pAPRRS and pSHE, respectively. The rescued mutant

and chimeric viruses were propagated in MARC-145 cells as described previously (Yuan and Wei, 2008).

Construction of plasmids

The subclone pCBSA, which contains the 5′ terminus (nt 1-2573) of the type 2 vAPRRS genome, was used as the shuttle plasmid vector for Quick-Change site-directed PCR mutagenesis during the reverse genetic manipulation (Lu et al., 2011). Two nucleotides, "at", were inserted between TRS and "AUG" to create the Nde I restrict endonulease site between the end of the 5′ UTR and the translation initiation codon of ORF1. The mutant fragment was transferred subsequently into the corresponding region of pAPRRS using Sph I in front of the T7 promoter and Afl II at nt 1688 in pAPRRS (Yuan and Wei, 2008). As a result, the mutant pTLNd4 was created. The Pac I restriction enzyme site was also created through the insertion of four nucleotides, "ttaa", ahead of TRS to create the mutant pPa2. These plasmids are shown in Fig. 1C. The primer pairs SFLNd/SRLNd and SFPac/SRPac used for PCR mutagenesis are listed in Table 1. pLVNd1 is a shuttle plasmid that was generated by truncating the genomic sequences in the full-length cDNA clone pSHE between the Not I site ahead of the CMV promoter and the Nde I site behind TRS, and was cloned into pBluescript SK+ vector. Following this, the 5′ UTR of type 2 clone pTLNd4 was replaced by that of the type 1 strain to construct the chimeric clone pTLV8 using these two restriction enzyme sites. All of the plasmids were verified by restricted enzymatic mapping and nucleotide sequencing (Shanghai Sunny Inc, China).

For the construction of converse chimeras pSHSP5, the pNSHE was used as the backbone in which a Nde I was inserted between the TRS and ORF1 translation initiation codon according to the pTLNd4 construction method. The vNSHE also showed similar virological characteristics to vSHE (Yuan et al., unpublished data), just like vTLNd4 to vAPPRS. Using Not I and Nde I digestion, the CMV promoter region and 5′ UTR of type 2 were substituted with that of type 1 in pNSHE backbone.

Splicing-overlap-extension (Liao et al., 2011) PCR was used to construct the chimeric clone revertants pTLV7823, 8401, 8914, and 9433. The restriction endonucleases used to transfer the mutant fragments into the related region in pTLV8 were Kpn I at nt 5388 bp, Pme I at nt 7800 bp, Avr II at nt 8959 bp and Xba I at nt 14772 bp. Throughout the study, pAS was used as a non-replicative plasmid control, as described previously (Lu et al., 2011).

Plasmid transfection and virus recovery

The parental plasmid pAPRRS and mutant plasmids pTLNd4, pPa2, pTLV8, pSHSP5 were isolated using a QIAprep Spin Miniprep kit as instructed (QIAgen, Hilden, Germany and identified further by spectrophotometry and 0.8% agarose gel electrophoresis (AGE).

Fig. 1. Nucleotide sequence alignment and prediction of the secondary structure of the 5′ UTR of type 1 and type 2 PRRSV strains, and diagram of mutant construction. (A) The Clustal V program was used to conduct nucleotide sequence alignment of the 5′ UTR of PRRSV strains including 5 type 1 strains and 11 type 2 strains. Nucleotides of inter-genotypically different domains were shaded gray and nucleotides in inter-genotypically conserved domains are shaded black. The 5′ UTR regions were designated artificially as the CS I, CS II, CS III, and CS IV domains. E and N denote type 1 and 2, respectively. SL1-5 denotes the stem–loop structures that exist in the 5′ UTR of the two genotypes, according to Mfold. LTH was contained in SL5, see Fig. 1B for details. TRS-L was in white and black shaded. (B) The RNA secondary structures of the 5′- proximal region of PRRSV genomes as predicted by Mfold program with the RNAviz modification. The displayed consensus type 1 (i), consensus type 2 (ii) represent the 5′-proximal 280 bp and 250 bp sequences, respectively. The TRS-L is shaded gray and the ORF1 translational initiation codon is shown in a box. The prominent stem–loops in dashed frames containing the LTH structures were inter-genotypically conserved, although the primary sequence identity of the two genotypes was low. (C) Schematic representation of mutation insertions between TRS, the initiation codon of ORF1 and PRRSV 5′ UTR. The sequences of PRRSV 5′ UTR, 3′ UTR, and the poly (A) tail are indicated. The mutants pTLNd4 and pPa2 were constructed from the PRRSV full length infectious cDNA clone pAPRRS using PCR-based mutagenesis. Nde I and Pac I were inserted between the TRS and the translational initiation codon of ORF1. Nucleotide sequences at the end of the 5′ UTR are shown in uppercase and the inserted nucleotides are shown in lowercase. The translational initiation codon of ORF1 (ATG) is in bold. The chimeric clone pTLV8 was obtained by replacing type 2 5′ UTR with type 1 5′ UTR, while pSHSP5 was contructed by replacing type 1 5′ UTR with type 2 counterpart, based on type 2 backbone. White bars denoted the sequence of type 2 and the hatched bar denoted the sequence of type 1. The parental pAPRRS was used as a control in all experiments. The top loops of the LTH in pTLNd4 and pPa2 were shown in (i) and (ii).

Table 1
Oligonucleotides used for RT-PCR mutagenesis, 5′RACE and Northern blotting analysis.

Name[a]	Sequence[b]	Position[c]	Application
SFND	5′-ATGACGTATAGGTGTTGGCTCTATGCCTTGACATTTG-3′	1–37	RT-PCR
SR2573	5′-CTGCCCAGGCCATCATGTCCGAAGTC-3′	2548–2573	RT-PCR
SFLNd	5′-GGTCTCTCCACCCCTTTAAC*cat*ATGTCTGGGATACTTGATCGGTGCACGTG-3′	170–219	PCR mutagenesis
SRLNd	5′-CACGTGCACCGATCAAGTATCCCAGACAT*at*GGTTAAAGGGGTGGAGAGAC-3′		PCR mutagenesis
SFPac	5′-TCTCTCCACCCCT*ttaa*TTAACCATGTCTGGGATACTTGATCGGTGCACG-3′	172–217	PCR mutagenesis
SRPac	5′-CGTGCACCGATCAAGTATCCCAGACATGGTTAA*ttaa*AGGGGTGGAGAGA-3′		PCR mutagenesis
SFLV101	5′-AGCCCAACAGGTATCCTTCTC-3′	100–121 (LV)	RT-PCR
SR683	5′-GGAGCGGCAGGTTGGTTAACACGTGA-3′	658–683	RT-PCR
SR343	5′-TAGCCCAACAGGTATCCTTCTC-3′	323–343	Nucleotide sequencing
SR1124	5′-CTTGCAGCCTCCGCTGTAGGTACTTGC-3′	1098–1124	5′RACE
SFLV1	5′-ATGATGTGTAGGGTATTCC-3′	1–19 (LV)	Nucleotide sequencing
SF2480	5′-CAGGGTGAACGGTAGAGCG-3′	2480–2503	Full-length nucleotide sequencing
SR4463	5′-CGTGGTGACAACCCAGAACAATG-3′	4444–4463	Full-length nucleotide sequencing
SF4344	5′-GCCCCGTCGGTCTCAGTCTTGCCATTTTT-3′	4344–4373	Full-length nucleotide sequencing
SR9753	5′-GTACCCGCACACTCTCGACTTCTTCCCCTCAT-3′	9722–9753	Full-length nucleotide sequencing
SF9348	5′-TCCCACCATGCCAAACTAC-3′	9348–9366	Full-length nucleotide sequencing
SR12013	5′-CCGATTCAAACCCCCAAGTATG-3′	11992–12013	Full-length nucleotide sequencing
SF11210	5′-TTTATAAGGCCACTGCCACC-3′	11210–11236	Full-length nucleotide sequencing
Qc	5′-CCAGTGAGCAGAGTGACGAGGACTCGAGCTCAAGC(C)$_{17}$-3′		5′RACE
Qo	5′-CCAGTGAGCAGAGTGACG-3′		5′RACE
Qi	5′-GAGGACTCGAGCTCAAGC-3′		5′RACE
Qst	5′-GAGTGACGAGGACTCGAGCGGCATGCTTTTTTTTTTTTTT-3′		Nucleotide sequencing, RT-PCR
SF12	5′-GTGTTGGCTCTATGCCTTGAC-3′	12–32	(−) gRNAs analysis, sg mRNA7 analysis
SR15284	5′-CTCCACAGTGTAACTTATCCTCC-3′	15261–15284	sg mRNA 7 analysis
SRLV378	5′-GCTTGTAAAACAAGCCAATTGCAG-3′	355–378(LV)	(−) gRNAs analysis
SRLV572	5′-TCACGAAGGTGTCGAGGAGCCAAGC-3′	548–572 (LV)	(−) gRNAs analysis
SRLV14835	5′-TCGATTGCAAGCAGAGGGAAC-3′	14815–14835(LV)	sg mRNA7 analysis
PLVR5	5′-GTACCCACGCCTCCAAGGTACACAAACACTAGAAGTGTCGTGTATGTAGGG-3′	20–70 (LV)	Probe for Northern Blot
PR3	5′-AATTTCGGCCGCATGGTTTTCGCCAATTAAATCTTACCCCCACACGGTCGC-3′	15470–15520	Probe for Northern Blot
F-actin	5′-CCCATCTATGAGGGCTACGC-3′		β-actin analysis
R-actin	5′-TTTGATGTCACGCACAATTTC-3′		β-actin analysis

Notes:

[a] Abbreviations in primer names: SF=forward PCR primer; SR=reverse PCR primer.

[b] Italic lowercase represents sequences different from vAPRRS.

[c] Numbers in the primer names denotes the nucleotide positions in the parental vAPRRS. LV represents the type 1 strain.

Samples of each DNA(3 μg), 15 μL of Lipofectamine™ LTX and 3 μL Plus Reagent (Invitrogen) were transfected directly into 70% confluent BHK-21 cells, according to the manufacturer's protocol. The cell supernatants were harvested at 24 h post transfection (hpt), aliquoted and stored at −80 °C, as P0. The P0 viral supernatants were used for passage in MARC-145 cells in six-well plates as virus stocks (five passages, P1–P5) for use in further experiments, as described previously (Sun et al., 2010; Yu et al., 2009; Yuan and Wei, 2008; Zheng et al., 2010).

Indirect immunofluorescence assay (IFA)

The BHK-21 cells were grown in six-well plates to 70% confluence, and each well was transfected by pAPRRS, pSHE, mutant clones and mock control to verify the expression of viral nucleocapsid protein (N), as reported previously (Gao et al., 2012; Sun et al., 2010). The cell monolayer was fixed at 24 hpt with ice-cold methanol for 10 min at room temperature and blocked subsequently with 0.1% bovine serum albumin (BSA) for 30 min, followed by incubation with a monoclonal antibody against the N protein of type 1 PRRSV (kindly provided by Ingenas Co., Madrid, Spain) and type 2 PRRSV (kindly provided by Dr. Ying Fang at South Dakota State University) at 1:600 dilution for 2 h at 37 °C. After five washes, the cells were incubated at 37 °C for 1 h with Alexa Fluor 568-labeled goat anti-mouse IgG (H+L) (Invitrogen). The fluorescence signal was visualized using an inverted fluorescence microscope (Olympus IX71), as described previously (Gao et al., 2012). For investigation of the viability of the mutant transfectants on BHK-21 cells, the anti-N IFA was repeated at 48 h post infection (hpi), using P0 viral supernatants from BHK-21 cells on the MARC-145 cell monolayer. The procedure is described in detail above and the cells were incubated at 37 °C for 1 h with Alexa Fluor 488-labeled goat anti-mouse IgG (H+L) (Invitrogen) (Gao et al., 2012).

5′ RACE, RT-PCR and full-length sequencing

For identification of mutant sites, genomic RNA was extracted from viral supernatants (P1–P5) using a QIAamp Viral RNA Mini Kit (QIAgen, Hilden, Germany) according to the manufacturer's procedure. Following this, the viral RNAs were used as the templates for RT-PCR. The primary transcription was conducted using avian myeloblastosis virus (AMV) reverse transcriptase (TaKaRa, Dalian, China) and primer SR2573 (Table 1). The cDNAs were synthesized with the forward primer pair SFND/SFLV101 and reverse primer SR683 (Table 1). The PCR parameters for vTLNd4 consisted of initial denaturation at 95 °C for 5 min followed by 30 cycles of denaturation at 95 °C for 30 s, annealing at 62 °C for 30 s and extension at 72 °C for 3 min. Similarly, the PCR procedure for vTLV8 consisted of initial denaturation at 95 °C for 5 min followed by 30 cycles of denaturation at 95 °C for 30 s, annealing at 58 °C for 30 s and extension at 72 °C for 45 s. The PCR products were loaded in 1% agarose gels for electrophoresis and purified subsequently using a QIAquick PCR purification kit (QIAgen, Hilden, Germany) according to the manufacturer's instructions. The purified PCR products were used directly as templates for sequence analysis and PCR restriction enzyme mapping.

The extracted viral RNAs (P1–P5) were also subjected to full-length sequencing. The RNAs were eluted with DNase/RNase-free water, quantified using NanoDrop® ND-1000 (Thermo Fisher Scientific), aliquoted and stored at −80 °C until use. The gRNAs

were reverse transcribed using the primer Qst (Table 1), and the cDNAs were used as templates for amplification of five overlapping genomic fragments using the primers RF1 (SFLV1/SR2573), RF2 (SF2480/SR4463), RF3 (SF4344/SR9573), RF4 (SF9348/SR12013), and RF5 (SF11210/Qst) (Table 1). The PCR products were purified by 1% agarose gel electrophoresis and cloned into the Zero Blunt® II-TOPO® PCR vector (Invitrogen) for sequence analysis. The resultant nucleotide sequences were assembled by SeqMan and aligned using the Lasergene® software package (Lu et al., 2011).

The 5′ end sequences of vTLV8 and vAPRRS (P1–P5) were also detected by 5′ RACE (Yuan et al., 2001). Total viral RNAs were extracted from infected cells using TRIzol® reagent (Invitrogen) and stored at −80 °C. Samples of viral RNAs (100 ng) were used for the transcription using avian myeloblastosis virus (AMV) reverse transcriptase (TaKaRa, Dalian, China) and primer SR2573. The reverse-transcribed PCR products were purified using a QIAgen purification kit (QIAgen, Hilden, Germany) according to the manufacturers instructions. The cDNAs were eluted in 40 µL of DNase/RNase-free water. Poly(G)-tailing (TaKaRa, Dalian, China) was conducted on the 3′-terminal of purified cDNA using a terminal deoxynucleotide transferase (New England Biolabs, USA). After this, the PCR products were eluted in 60 µL ddH$_2$O and stored at −30 °C for further use. First round PCR was completed as described previously (Yuan et al., 2001) using 2 pM Qc and 10 pM Qo as the forward primers and 10 pM SR1124 as the reverse primer. The first round PCR was performed using the primer pair Qi and SR683 and initial denaturation at 95 °C for 5 min followed by 30 cycles of denaturation at 95 °C for 30 s, annealing at 58 °C for 30 s and extension at 72 °C for 60 s. An identical second round of PCR was then performed using 1 µL of the first round PCR product; the parameters were initial denaturation at 95 °C for 5 min followed by 30 cycles of denaturation at 95 °C for 30 s, annealing at 55 °C for 30 s and extension at 72 °C for 40 s. After electrophoresis in 1% agarose gels, the PCR products were purified using a QIAquick gel- purification kit (QIAgen, Hilden, Germany) according to the manufacturer's protocol. The purified PCR products were used directly as templates for subcloning and nucleotide sequencing.

Analysis of (-) gRNAs and sg mRNAs

Total RNAs were extracted from transfected BHK-21 cells using TRIzol® reagent (Invitrogen) and dissolved in DNase/RNase-free water. Removal of input DNA from RNA preparations was conducted by incubating with DNase I at 37 °C for 30 min according to the protocol of the DNA-free kit (Ambion). The purified RNAs were used as the templates in RT-PCR for detection of (-) gRNAs and sg mRNAs. A house-keeping β-actin mRNA was used as the internal control, as reported previously (Lu et al., 2011). The PCR products were quantified using Quantity One® 1-D analysis software version 4.6.2. The wild type virus vAPRRS was set to be 100%.

The forward primers SF12 and SFLV1 were used for cDNA synthesis from 2 µg of total RNAs using SuperScript TM II Reverse Transcriptase (Invitrogen. The first strand cDNA was treated with 2 µg RNase A (Ambion) at 37 °C for 30 min to eliminate the remnant RNA. The RNase A activity was removed by heating at 95 °C for 10 min. Samples of cDNA (2 µL) and the primer pairs SF12/SR683, SFLV101/SR683, SFLV101/SRLV572 and SF12/SRLV572 were prepared for the first round PCR. The reaction parameters consisted of initial denaturation at 95 °C for 30 s followed by 30 cycles of denaturation at 95 °C for 30 s, annealing at 58 °C for 30 s and extension at 72 °C for 30 s. The nested PCR was conducted using 2 µL 1000-fold diluted primary PCR product and primer pairs SF12/SR343, SFLV101/SR343, SRLV101/SRLV378

and SF12/SRLV378. The PCR cycle parameters were the same as above.

Subgenomic mRNA7 of the mutant viruses was amplified by the leader–body junction RT-PCR (Lu et al., 2011; Zheng et al., 2010) using TaKaRa AMV and LA Taq (TaKaRa, Dalian, China). The reverse primer Qst was used for the RT reaction, and the four primer pairs SF12/SR15284, SFLV1/SR15284, SFLV1/SRLV14835 and SF12/SRLV14835 were used for detection of sg mRNA7. The reaction parameters consisted of initial denaturation at 95 °C for 5 min followed by 30 cycles of denaturation at 95 °C for 30 s, annealing at 63 °C for 30 s and extension at 72 °C for 30 s. All PCR products were gel purified using a QIAquick gel- purification kit (QIAgen, Hilden, Germany), and subsequently subcloned and sequenced.

Titration of rescued viruses

The first round rescued viruses from transfection of BHK-21 cells were titrated in MARC-145 cells. The viral titers (TCID$_{50}$ mL^{-1}) were determined as described previously (Gao et al., 2012). Each of the viral titrations was repeated three times, and the results shown in the figures indicated the mean value.

To determine the growth dynamics, MARC-145 cells in six-well plates were infected with all of the mutant and wild type viruses (P1) at 0.01 MOI, as described previously (Lu et al., 2011; Sun et al., 2010; Yu et al., 2009). After 1 h of adsorption, the cell monolayers were washed. Supernatants (200 µL) were harvested at the indicated time points and frozen at −80 °C until use. Viral titration was conducted by quantitation of viral plaques on MARC-145 cells (Sun et al., 2007; Yu et al., 2009).

Viral plaque assay

MARC-145 cells in six-well plates were infected with 200 µL of 10-fold serially diluted P1 viruses. The plates were incubated at room temperature for 1 h. Following this, cell monolayers were washed with PBS and overlaid with 1% low melting agarose in MEM (Invitrogen) containing 2% FBS. The agarose solidified plates were inverted (placed top down) placed in a 5% CO$_2$ incubator and incubated at 37 °C. The cell monolayers were stained at 5 days post infection (dpi) with 5% crystal violet in 20% ethanol (Gao et al., 2012).

Viral RNA isolation and Northern blotting

MARC-145 cells were infected with vTLV8, vTLNd4 and vAPRRS (P5) at MOI of 0.01. Total RNA from each sample was isolated at 36 hpi using a QIAgen RNeasy Mini kit (QIAgen, Hilden, Germany). Samples of total RNA (5 µg) were loaded and separated by 1% formaldehyde-denatured agarose gel electrophoresis (AGE). The separated total RNA was transferred to a BrightStar-Plus membrane (Ambion) for 8 h, and cross-linked by UV light for 15 min. Pre-hybridization was performed at 42 °C for 30 min followed by detection using the genotype-specific 3′ UTR or 5′ UTR oligodeoxynucleotide probe PR3/PLVR5 (Table 1). Blots were hybridized for 12 h and washed with low-stringency and high-stringency buffers, blocking buffer and wash buffer according to the manufacturer's instructions (Ambion). The filters were incubated with alkaline phosphatase-conjugated streptavidin followed by reaction with the chemiluminescent substrate CDP-STAR (Ambion). The overlaid films were obtained by exposure for 12 h in a dark cassette box in a dark room.

Prediction of RNA secondary structure

The RNA secondary structures were predicted using the energy minimization program of Mfold server (http://frontend.bioinfo.rpi.edu/applications/mfold/cgi-bin/rna-form1-2.3.cgi) (Zuker, 2003) and edited using the secondary structure drawing and modifying software RNAviz version 2 (De Rijk et al., 2003).

Results

Conserved domains exist in the 5′ UTR of type 1 and 2 PRRSVs and their secondary structures have similar feature

Five type 1 PRRSV strains (GenBank accession Nos. M96262, DQ489311, AY366525, EU076704 and AY588319)t and eleven type 2 PRRSV strains (GenBank accession Nos. AY150564, GQ330474, EF488048, EF112445, AF184212, EU109503, EU200962, U87392, EF112447, AY424271, and AF331831) were compared and aligned for their 5′ UTR sequences using DNAstar software. The sequence alignment is presented in Fig. 1A. The 5′ UTR sequence of type 1 PRRSV strains is 30 nt longer than that of type 2 strains. The nucleotide consensus sequence in the 5′ UTR regions was identified for type 1 and type 2 strains and is boxed in Fig. 1A, designated as CS I, CS II, III and IV. The high-order structures of the PRRSV 5′ UTR were analyzed using the Mfold program, followed by modification using the RNAviz software. The predicted secondary structures of the type 1 and type 2 PRRSV 5′ UTR are shown in Fig. 1B (i) and (ii). They were characterized by six major putative helical stem–loops, which we arbitrarily designated as ESL1-5 for type 1 PRRSV and N-SL1-5 for type 2 PRRSV, respectively (Fig. 1B i and 1B ii). The E-SL1 in type 1 PRRSV could be separated into two minor stem–loops, designated as E-SL1a and E-SL1b, which corresponded to N-SL1 in type 2 PRRSV. Similarly, NSL4 in type 2 PRRSV also could be divided into two minor stem–loops, named N-SL4a and N-SL4b, which corresponded to E-SL4 in type 1 PRRSV (Lu et al., 2011). Although the primary nucleotide sequences of these strains showed low sequence homology, their RNA secondary structures were similar, especially the most important leader TRS hairpin (LTH) parts, as shown by the shaded grey box in Fig. 1B, that is, the prominent N/E-SL5.

Virus rescue, RNA synthesis and gene expression show quite different consequences for the mutants and the WT

pAPRRS, pSHE and the mutant cDNA clones, pTLNd4, pPa2, pTLV8 and pSHSP5 were transfected into BHK-21 cells, and subsequently used to infect MARC-145 cells for identification of viral infectivity. When passaged in MARC-145 cells, pTLNd4 and pAPRRS developed CPE at 3-4dpi. When approximately 80% cytopathic effect (CPE) had developed, viral supernatants from the infected MARC-145 cells were harvested and designated vTLNd4 and vAPRRS (P1), respectively. Both the transfected BHK-21 cell monolayers and infected MARC-145 cell monolayers were examined via IFA using MAb against two genotypes of PRRSV N protein. The results revealed that the similar N protein expression level for pAPRRS and pTLNd4 tranfected wells. Moreover, N protein expression of type 1 WT, pSHE, showed comparable level with that of type 2 WT. while only a few isolated spots were found in pTLV8 and pPa2 transfected wells, as shown in Fig. 2C. However, none of the fluorescent signal could be detected in pSHSP5 transfected well. When transfectant supernatants were used to infect MARC-145 cells, vTLV8 showed a subtly different IFA pattern from that of vAPRRS. However, mutant pPa2 and chimeric pSHSP5 did not develop CPE even after the fifth passage in MARC-145 cells. The IFA result showed that pPa2 developed a

PRRSV-specific fluorescent signal in a few of transfected BHK-21 cells but it did not show any infection of MARC-145 cells. N-specific fluorescent signal could not detected in pSHSP5 transfected BHK-21 cells and MARC-145 cells inoculated with supernatant collected from pSHSP5 transfected BHK-21 cells, as shown in Fig. 2C. To further confirm whether pSHSP5 was infectious, we repeated the transfection experiments using BHK-21 cells three more times and transferred the transfection supernatants to MARC-145 cells for three blind passages. No typical CPE were observed in the MARC-145 cells, and no viral genomic RNA was detected in either the total intracellular RNA or the culture supernatant by RT-PCR. This result suggested that the viral rescue of pPa2 and pSHSP5 did not occur in MARC-145 cells. Therefore, the insertion of the four nucleotides "ttaa" in front of TRS caused inactivation of the pPa2, while "at" insertion between TRS and translational initiation codon of ORF1 did not affect the production of infectious progeny virus.The replacement of 5′ UTR of type 2 with 5′ UTR of type 1 in the context of type 2 PRRSV clone did not affect virus viability. Otherwise, the converse replacement in a context of type 1 PRRSV was lethal.

For the negative strand gRNA ((−) gRNA) RT-PCR analysis, in order to detect whether the possible interferences from the input DNA and the RNA transcript generated by the CMV promoter, the RNAs extracted from pAS and WT transfected cells were used for RT-PCR, as our previously reported (Lu et al., 2011). The results in Fig. 2A showed that DNase I and RNase A could eliminate transfected input DNAs and the CMV-driven RNAs. Therefore the presence of the newly synthesized viral (−) gRNA could be detected. The results of the analysis of (−) gRNA and sg mRNA7 are shown in Fig. 2B. RT-negative controls were also performed for all of the clones. After DNase I and RNase A digestion, nothing could be detected by the RT-PCR (data not shown). The levels of RNA synthesis levels of vTLNd4 showed almost no difference from those of WT. Otherwise the level of chimeric vTLV8 was reduced compared with vAPRRS. Remarkably, the level of RNA synthesis of the mutant pPa2 showed great similarity to that of pAPRRS, although it did not develop CPE in the tested cell cultures. For pSHSP5, (−) gRNA could also be detected, but the synthesis level was largely reduced compared with pSHE, as shown in Fig. 2B. The leader–body junction PCR was performed for identification of sg mRNA7, using four primer pairs as follows, SF12/SR15284, SFLV1/SR15284, SFLV1/SRLV14835 and SF12/SRLV14835. The sg mRNA7 transcription level of vTLV8 dropped to 50% compared with pAPRRS, Otherwise, the sg mRNA7 could not be detected in pSHSP5 transfected cells, indicated that the sg mRNA transcription was dramatically impaired. Taken together, the results indicated that 5′ UTR of type 1 PRRSV substitution did not affect type 2 PRRSV propogation in MARC-145 cells. The Chimera pTLV8 shared almost the similar RNA synthesis level and virological characteristics with the parental type 2 PRRSV strain, vAPRRS. However, the converse chimera pSHSP5, in which 5′ UTR of a type 1 PRRSV was substituted with counterpart of the type 2 PRRSV, was lethal. Although the (-) gRNA replication could be detected, the replication level was significantly impaired and the sg mRNA transcription was absolutely abolished. Therefore, the type 1 5′ UTR replacement could allow maintain fully functional activities of type 2 PRRSV.

The virological properties and sg mRNA transcription level of vTLV8 are indistinguishable from those of the parental virus

The chimeric virus vTLV8 and the other mutants were compared with the parental virus vAPRRS with regard to their titers, plaque morphology and growth profiles in MARC-145 cells. After 48 hpt in BHK-21 cells, the supernatants were harvested and used to infect MARC-145 cells for measurement of their titers. The
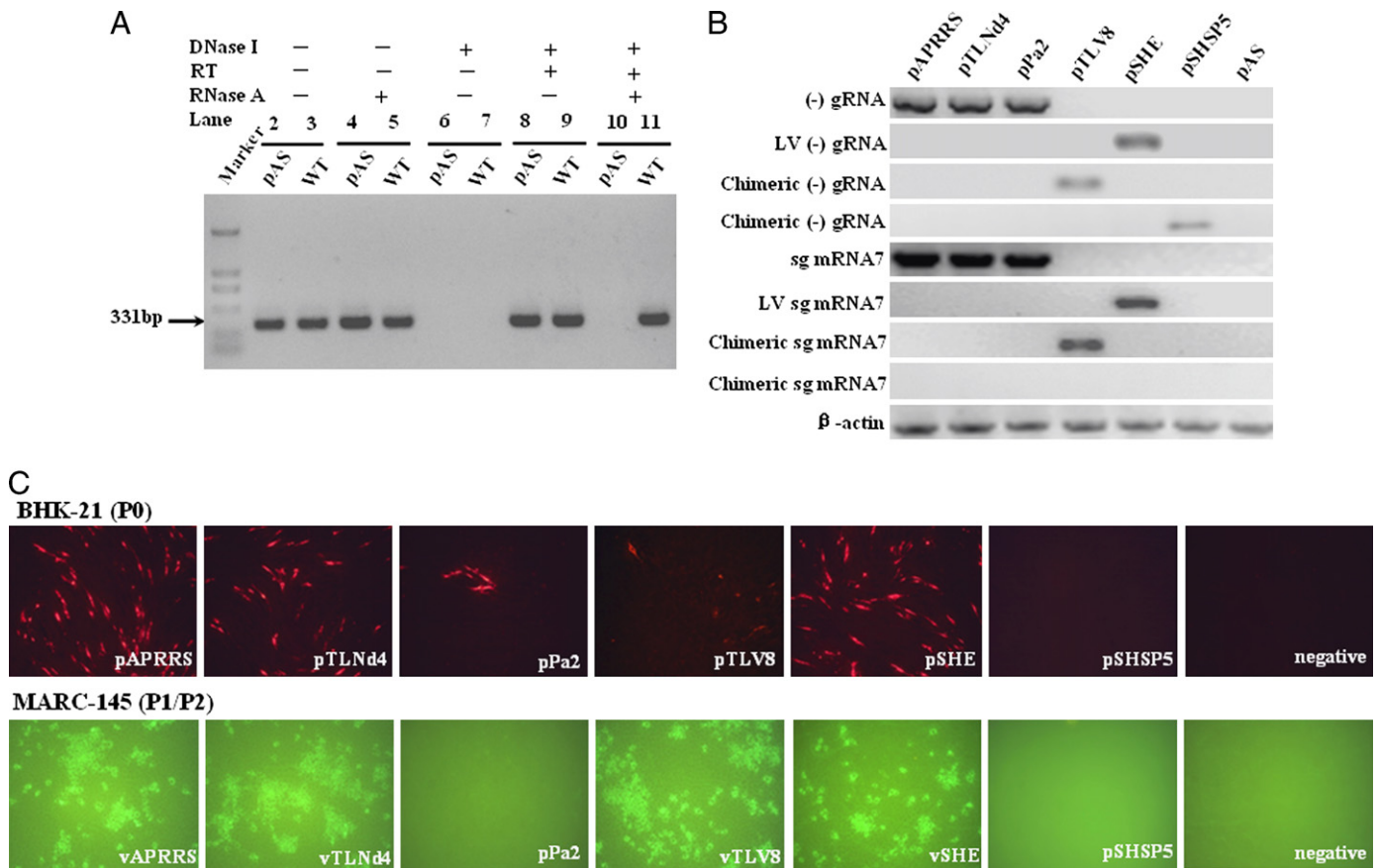
Fig. 2. Analysis of RNA transcription levels. (A) RT-PCR of RNAs isolated from non-replicative control pAS and WT transfected cells. DNase I and RNase A were used to eliminate the possible interferences. The nested primers used were listed in Table 1. A molecular size marker was a 2-kb ladder. The number of the lanes was indicted. (B) Semi-quantitative RT-PCR analysis of the mutant PRRSVs. Total cellular RNAs were extracted from transfected from BHK-21 cells at 24 h post transfection. β-Actin was used as an internal control for transcription level, and pAS was used as an unreplicative control, in which the genes ORF1a and ORF1b were absent. RT-negative controls were also performed for all of the clones, but did not show in the figure, due to the space limit. (C) Indirect immunofluorescence assay of the transfected BHK-21 cells and infected MARC-145 cells. The cell monolayers were fixed at 24 h post inoculation and stained with monoclonal antibody against N protein.

results shown in Fig. 3A illustrate that the viral titer of the parental virus vAPRRS was $1 \times 10^{3.67}$ TCID$_{50}$/mL while the chimeric virus vTLV8 did not develop CPE in the first passage in MARC-145. The viral titer of the mutant vTLNd4 was $1 \times 10^{2.23}$ TCID$_{50}$/mL. In addition, the mutant pPa2 did not develop CPE. There were no differences in viral plaque morphology between vTLV8, vTLNd4, and vAPRRS, as shown in Fig. 3C. Although vTLV8 did not develop CPE in the first passage, the analysis of growth kinetics showed that vTLV8 had almost the same propagation state as vTLNd4 and vAPRRS (Fig. 3D).

In order to analyze the sg mRNA profiles of the MARC-145 cells infected by the mutant viruses, total intracellular RNAs were extracted from the P5 viral supernatants for Northern blotting analysis. The specific oligonucleotide biotin-labeled probes against type 2 PRRSV 3′ UTR (PR3) and type 1 PRRSV 5′ UTR (PLVR5) were designed to hybridize with the viral RNA. The sequences of the probes are displayed in Table 1. The results demonstrated that the sg mRNAs of chimeric vTLV8 were recognized by both probes, and the sg mRNA7 was most abundant during the viral transcription process, as shown in Fig. 3B. The parental vAPRRS and mutant vTLNd4 were reacted with the type 2-specific probe PR3, not the type 1-specific probe PLVR5.

Replacement of complete type 2 5′ UTR retains fully functional activities and genetically stable

To confirm that the mutant viruses contained the specific mutations in the 5′ UTR, mutant sites were detected via RT-PCR

and the 5′-proximal sequences were identified by 5′ RACE. The results showed that the *Nde* I site was present in the mutant viruses, and the authentic type 1 5′ UTR sequence was maintained in vTLV8 throughout five serial passages (P1–P5). The mutants were genetically stable, as shown in Fig. 4.

The effect of *Nde* I insertion on sg mRNA transcription for vTLNd4 and vTLV8 was also investigated. sg mRNAs 7.1 and 7.2 for vTLNd4 were detected by leader–body junction RT-PCR (Lu et al., 2011; Zheng et al., 2010). Nucleotide sequence analysis of each RT-PCR product revealed that the sg mRNA7 level of vTLNd4 was identical to that of the parental vAPRRS, which indicates that the insertion of *Nde* I had no impact on the viral mRNA transcription of the mutant (data not shown. The sg mRNA-specific RT-PCR for vTLV8 detected the sg mRNAs 2, 3, 4.1, 5.1, 6.1, 7.1 and 7.2. Comparison of the nucleotide sequences illustrated that the leader–body junction sites of vTLV8 were conserved with their counterparts in the parental vAPRRS (data not shown). There was no dramatic difference in the Northern blotting profiles between the WT, vTLNd4 and vTLV8, as shown in Fig. 3B. Taken together, these results show that the mutations did not produce an evident effect on viral sg mRNA transcription.

Type 1 5′ UTR chimeric mutant possesses nucleotides mutations in the nsp9 region

The chimeric vTLV8 and vAPRRS genomic sequences were subjected to full-length sequencing analysis. When compared with the parental vAPRRS, there were no other nucleotide
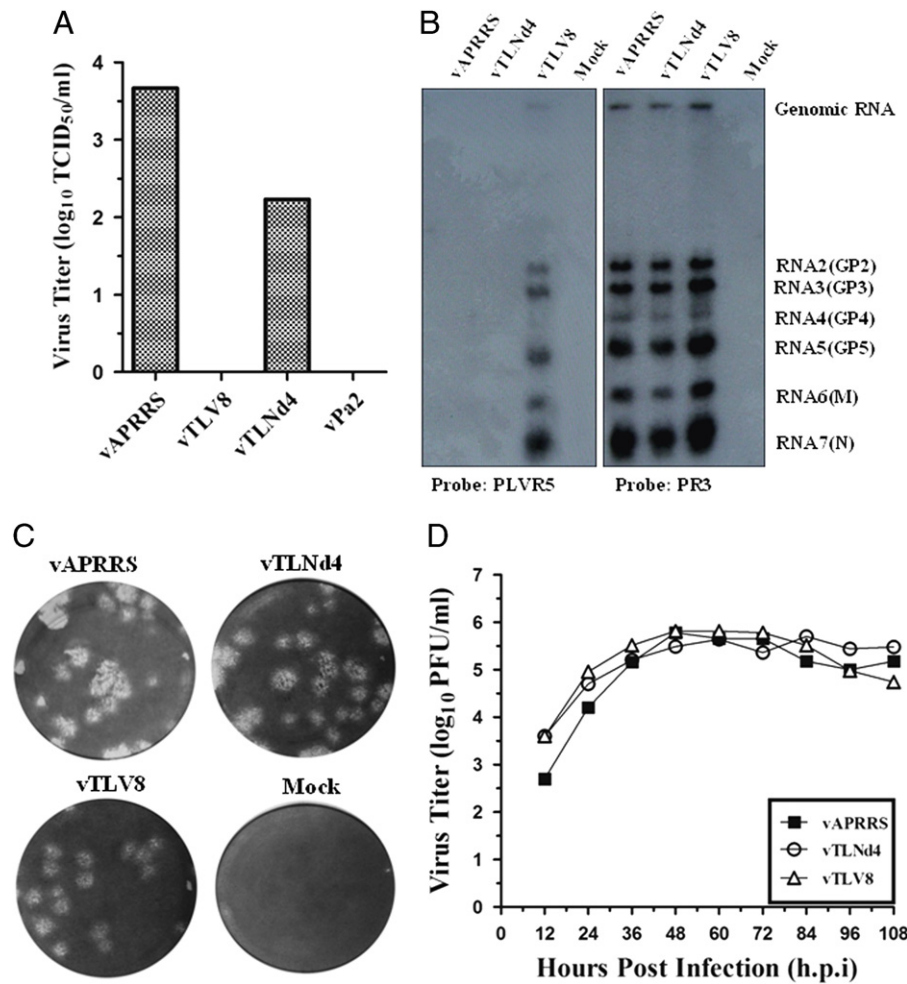
Fig. 3. Comparison of the growth comparison of wild type and mutant viruses. (A) Measurement of viral titers (TCID$_{50}$/mL) of transfected BHK-21 cells. The transfectant supernatants were collected from BHK-21 cells at 36 h post transfection and used to infect MARC-145 cells for determination of titers. (B) Viral RNA transcription levels were detected by Northern blotting. Fresh MARC-145 cell monolayers were infected with vTLNd4, vTLV8, and parental vAPRRS at MOI of 0.01. Intracellular RNAs were extracted at 36 h post transfection. The RNAs were separated on 1% agarose gels, blotted onto a nitrocellulose membrane (Ambion), and then probed subsequently with type 1 5′ UTR-specific probe PLVR5 and type 2 5′ UTR-specific probe PR3, respectively. Genomic RNA and subgenomic mRNAs 2 to 7 are shown. (C) Plaque morphology. The MARC-145 cells in six-well plates were infected with the rescued viruses vAPRRS, vTLNd4, and vTLV8. The mock control represented non-infected MARC-145 cell monolayers. The MARC-145 cells were stained with crystal violet 6 days post infection. (D) Growth curves. The MARC-145 cells were infected with the fifth passage of the rescued viruses vAPRRS, vTLNd4 and vTLV8 at MOI of 0.01. Viral supernatants were harvested at the indicated times and titers were determined by plaque assay on MARC-145 cells.

mutations except for five nucleotide substitutions that occurred in the RdRp coding region (nsp9) in vTLV8, which caused four amino acid mutations: T7823C caused the amino acid change Leu→Ser, A8401T caused Thr to change to Ser, A8914T caused Ile to change to Phe, and A9433T caused Ile to change to Phe.

In an attempt to address the function of these amino acid mutations, we introduced four nucleotide mutations (T7823C, A8401T, A8914T, and A9433T) into the backbone of pTLV8 in order to obtain the revertants pTLV7823, 8401, 8914, and pTLV9433. In contrast to pTLV8, the four revertant viruses could be rescued from the first passage in MARC-145 cells using the transfection supernatants in BHK-21 cells. Subsequently, we examined genomic RNA replication and sg mRNA7 transcription levels, together with N protein expression, in transfected BHK-21 cells. The results are shown in Fig. 5. Similar levels of sg mRNA7 transcription were found in these four revertants to those in the parental vAPRRS, but not in vTLV8. If the negative strand genomic RNA replication level of vAPRRS was set at 100%, the relative percentages for vTLV7823, vTLV8401, vTLV8914, and vTLV9433 were 60%, 83%, 71%, and 79%. The level of expression of the PRRSV N-protein of these four revertants showed subtle differences from

WT, as shown in Fig. 5C. To test the infectivity of these revertant viruses, the supernatants of the transfected BHK-21 cells at 48 hpt were harvested for first cycle viral titration in MARC-145 cells. The viral titer for WT was $1 \times 10^{3.67}$ TCID$_{50}$ mL^{-1}, while those of the revertants vTLV7823, vTLV8401, vTLV8914, and vTLV9433 were $1 \times 10^{1.23}$ TCID$_{50}$ mL^{-1}, $1 \times 10^{1.5}$ TCID$_{50}$ mL^{-1}, 1×10^{1} TCID$_{50}$ mL^{-1}, and $1 \times 10^{1.33}$ TCID$_{50}$ mL^{-1}, as shown in Fig. 6A. Although the growth properties of the four mutant viruses were reduced in comparison with the WT, vAPRRS, they could be rescued during the first passage process (P1). Otherwise vTLV8 could not be recovered in P1.

The plaque morphology of these viruses was also assessed, and the results showed that the plaques of the mutant viruses were distinctly different from those of WT in both morphology and numbers when all using 0.01 MOI. The plaque number of vTLV8 was the lowest, and the plaque size was moderate. The viral titer of vTLV8401 manifested by the plaque assay was consistent with that of the first cycle viral titration. The plaque size was the largest and relatively uniform, while vTLV7823 had a very uneven plaque size. The plaque number of vTLV8914 was relatively low, as shown in Fig. 6B.

Fig. 4. Confirmation of nucleotide sequences of the rescued viruses. (A) Nucleotide sequencing of the rescued viruses. To determine whether the chimeric mutation was retained in the vTLV8 of P1 through P5, the specific domain was amplified as described in the Materials and Methods. Alignment of nucleotide sequences showed that a chimeric region existed in the rescued viruses. A dot (.) denotes identical sequences when compared with the parental vAPRRS. The inserted *Nde* I restriction enzyme site is underlined. Nucleotide variations are shaded in gray. The sequence displayed in the upstream box shows that the 5′ UTR of chimeric vTLV8 was homologous with that of the type 1 strain (M96262), while the downstream box indicates that the sequence following the 5′ UTR of vTLV8 was identical to that of type 2 vAPRRS (GQ330474). (B) The truncated trace files of nucleotide sequences of vAPRRS and vTLV8. The 54-bp authentic 5′-proximal sequences of vTLV8 are shown behind the poly (C).

Fig. 5. Mutational analysis for revertant chimeric viruses and vTLV8. (A) Semi-quantitative RT-PCR analysis of vTLV8 and revertants. Total cellular RNAs were extracted from mutant plasmids-transfected BHK-21 cells at 24 h post transfection. β-Actin was used as an internal control and pAS as an unreplicative control. (B) Semi-quantitative analysis of the relative abundance of the negative-strand genomic RNAs and sg mRNAs in transfected BHK-21 cells. The RT-PCR products presented in (A) were quantified by using the Quantity One 1-D analysis software version 4.6.2. The transcription level of the parental vAPRRS was set at 100% and the mock value was subtracted. (C) Indirect immunofluorescence assay. The infected MARC-145 cell monolayers were fixed at 24 h post infection and stained with monoclonal antibody against N protein.

Discussion

PRRSV has evolved into a distinct European genotype 1 and a North American genotype 2. Types 1 and type 2 PRRSV share only 60% identity of their overall nucleotide sequences; they are two very distinct genotypes (Murtaugh et al., 1995; Nelsen et al., 1999). However, the two types retain similar genomic organization (Meng et al., 1994; Meulenberg et al., 1993a; Murtaugh et al.,

1995; Nelsen et al., 1999). PRRSV continues to evolve rapidly by random genetic mutation and intragenic RNA recombination. Genetic divergence exists between geographically and temporally separate isolates (Matanin et al., 2008).

The 5′ UTR of many positive-stranded RNA viruses, including PRRSV, has been demonstrated to contain *cis*-acting elements required for viral replication and sg mRNA transcription (Liu et al., 2009). In equine arthritis virus (EAV) sg mRNA transcription

Fig. 6. Characterization of revertant viruses. (A) Detection of viral titers in transfected BHK-21 cells with four revertants: vTLV7823, vTLV8401, vTLV8914, and vTLV9433. The parental vAPRRS and chimeric vTLV8 were included for comparison. The transfectant supernatants were collected from BHK-21 cells at 36 h post transfection and then used to infect MARC-145 cells for determination of $TCID_{50}$/ml. (B) Plaque morphology. The MARC-145 cells in six- well plates were infected with the viruses (P1) and stained with crystal violet at 6 days post infection.

(Born et al., 2005); (Van Den Born et al., 2004), a short, conserved leader transcription-regulating sequence (TRS-L) is located in the loop of one hairpin structure (LTH) of the 5′ UTR and downstream body TRS (TRS-B). A similar LTH structure could be predicted for the 5′-proximal region of all arterivirus genomes (van Marle et al., 1999), and also for many coronaviruses (Lu et al., 2011; Van Den Bornet al., 2004). It is a key element in discontinuous sg mRNA synthesis (Bornet al., 2004). In this study, the secondary structure models for the 5′-proximal sequences of the two PRRSV genotypes were obtained using the energy minimization program on the Mfold web server. The 5′ UTR of the two genotypes of PRRSV showed only 60% genetic identity. However, according to the structure model predicted by the Mfold website server and in silico analysis, their predicted secondary structure reveals a certain degree of similarity, especially in the top loop of the striking hairpin structure in which TRS is located, the counterpart of the EAV LTH. Compared with the structural models for the PRRSV and EAV 5′-terminal regions, we found that there were more stem–loop (SL) structural elements in the EAV 5′-terminus than that of PRRSV. The LTH of PRRSV was more striking than its counterpart in EAV. The single strand region of the 5′-proximal region of EAV is longer than that of PRRSV. The top loop of the EAV LTH, which was considered to make the leader TRS accessible as an acceptor during template switching, is larger than the top loop of PRRSV LTH. Despite the lack of identity at the level of primary sequence, the two 5′ UTRs are high-ordered and both contained LTHs, which might be considered to be an independent RNA signal in sg mRNA synthesis. Given that thermodynamic algorithms do not show 100% accuracy in the prediction of RNA secondary structure, phylogenetic analysis remains a useful tool for the establishment of structure models. In a study of the 5′-proximal sequence of EAV, van den Born el al. used chemical and enzymatic probing to gain experimental evidence. The combined results of the chemical and enzymatic probing were in good agreement with the structure mode (Van Den Bornet al., 2004).

In this study, we entered the 260-bp sequence of pTLV8 and 260-bp sequence of pSHSP5 into the Mfold software, and the RNA secondary structures obtained showed that, although the secondary structure of chimeric pTLV8 and pSHSP5 had changed dramatically compared with each other and the two structures displayed in Fig. 1B, The TRS location of the two chimeras were quite different. The TRS of pTLV8 was still located in the prominent top loop of LTH structure, as shown in Fig. 7A, but the TRS of pSHSP5 was no longer located in the prominent top loop structure (Fig. 7B). pTLV8 and pSHSP5, the two chimeric mutant viruses rescue showed different results. pTLV8 was viable, while pSHSP5 was lethal. The results indicated that the secondary structure of TRS and its adjacent sequences would be very important for viral replication and infectivity. The viral properties of pTLNd4 were identical with those of the WT, while pTLV8 could be rescued during the second passage process (P2 and pPa2 could not be rescued even after five attempts of transfection and passages). The predicted secondary structure for pTLNd4 was compared with that of pPa2. The predicted top loops of pTLNd4 and pPa2, which contain the TRS are shown in detail in Fig. 1C (i) and (ii). The addition of the nucleotides "at" or "ttaa" to pTLNd4 and pPa2 had different consequences. The intermediate mutant pTLNd4 almost retained the original structure when compared with the parental pAPRRS, while the sequence "UUAACC AUG" in pPa2 did not fold into the prominent hairpin loop of LTH, as shown in Fig. 1C (i) and (ii). This demonstrated that the insertion of the nucleotides "at" between TRS and the first coden of ORF1 did not cause changes in the LTH and thus had no adverse effect on viral infection. We also produced related mutations aimed at the conserved prominent SL structure, containing insertion, deletion and substitution and demonstrated that the conserved top loop structure and its authentic primary sequence were essential for viral replication function (data not shown). Therefore, we propose that the key element in the LTH is the top loop in which TRS is located.

The viral titers of four revertant viruses were higher than those of the parental chimeric virus and the plaque size differed from that of the chimeric vTLV8. The results of the semi-quantitative RT-PCR showed that the level of RNA synthesis in the four mutant viruses was higher than for vTLV8. Taken together, the results show that the regulatory function of the 5′ UTR is related closely with RdRp; the heterologous 5′ UTR with revertant RdRp played a joint role in the process of virus rescue.

It had been demonstrated that SL2 in the 5′ UTR of type 2 PRRSV could be replaced with its counterpart from a type 1 PRRSV (Lu et al., 2011). We found, further that the complete 5′ UTR of type 2 PRRSV could be replaced with its counterpart from type 1 PRRSV as the promoter for virus replication in the type 2 virus backbone. Therefore, we postulate that the high-ordered structure is more important than the primary sequence in maintaining viral function. Nevertheless, the RNA structural model obtained from in silico analysis must be examined in experimental studies.

RNA-dependent RNA polymerase (RdRp) is an enzyme that catalyzes the replication of RNA from an RNA template. It is an
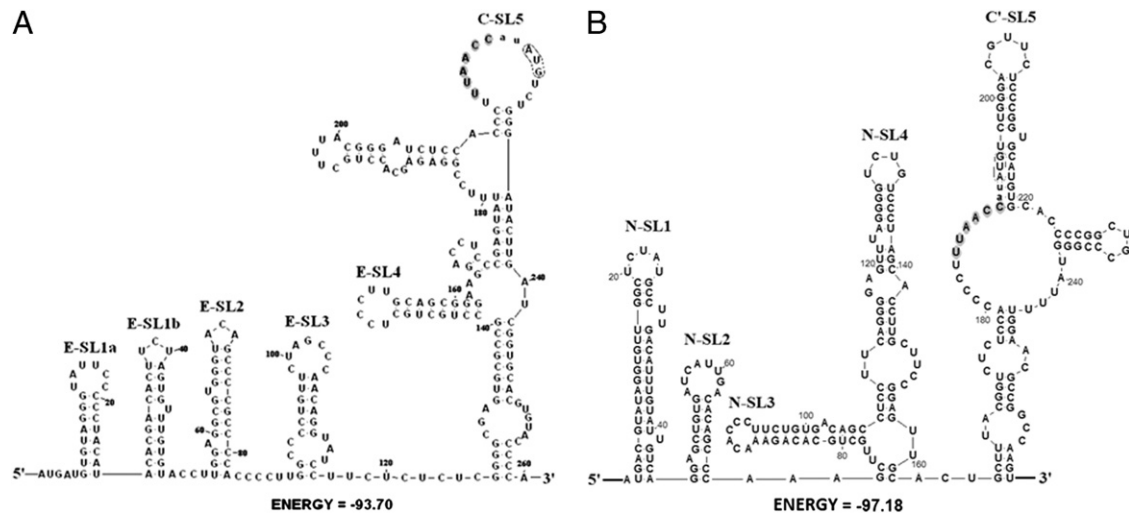
Fig. 7. Schematic representation of secondary structures which predicted by Mfold program from 5′ UTR swapping mutants. (A) The secondary structure of the 5′- proximal 280 bp of chimeric pTLV8 was displayed, the TRS-L was shaded gray and the ORF1 translational initiation codon was shown in box. "E" denoted European type (type 1), "C" denoted chimeric. (B) The secondary structure of the 5′- proximal 260 bp of chimeric pSHSP5 was shown, the TRS-L was also shaded gray and "AUG" was shown in box. "N" indicated North American type (type 2), "C′" also indicated chimeric.

essential protein encoded in the genomes of all RNA-containing viruses with no DNA stage that have sense-negative RNA, it catalyzes the synthesis of the RNA strand complementary to a given RNA template. The RdRp region of PRRSV is located in Nsp9 (Fang and Snijder, 2010), which is encoded in ORF1b. RdRp and RNA helicase (Hel; Nsp10) are important elements of the viral replication and transcription complex (RTC); the RTC mediates both genome replication and the synthesis of a discontinuous nested set of sg mRNAs. Present research has revealed that viral RdRp plays a function in the viral life cycle, tightly associated with the 5′ UTR and 3′ UTR. Stem–loop A (SLA) located in the Dengue virus (DENV) 5′ UTR provides the binding site for RdRp. Viral genomic synthesis is initiated from the viral 3′ end of the viral genome through a process of cyclization, using 5′ binding RdRp (Filomatori et al., 2006). It was reported an important cooperative interaction among chimeric hepatitis C/GB virus B NS5A (RdRp), 5′ UTR, and 3′ UTR in viral replication (Warter et al., 2009). Such an interaction is crucial for viral RNA replication, packaging, and virion assembly in the viral life cycle. In this study, on the based of reverse genetic manipulation of heterogeneous UTR swapping in an infectious cDNA clone of type 2 PRRSV, it was found that substitution of type 1 5′ UTR caused several revertant mutation sites to occur in the RdRp region. The chimeric pTLV8 could be recovered during the second passage process (P2), but the revertants pTLV7823, 8401, 8914, 9433 could be rescued only in P1. The results of the analysis of N protein translation level, semi-quantitative RT-PCR and Northern blotting analysis showed that the level of RNA synthesis of the four mutant viruses were higher than that of vTLV8. Viral plaque assay and titration indicated that the vitality of the revertant viruses was greater than that of vTLV8. Taken together, the results show that the regulatory function is closely related to RdRp, and the heterologous 5′ UTR with revertant RdRp played a joint role in the process of virus rescue.

The functional studies reported here provide additional data that increase our understanding of the role of the 5′ UTR in the regulation of PRRSV RNA replication, and sg mRNA transcription and translation. For the prevention of PRRSV infection, many regulatory mechanisms in the viral life cycle need to be elucidated.

The research on heterogeneous UTR substitution is scarce, especially for PRRSV. Kang et al. (2006) found that the three SL

structures in severe acute respiratory syndrome coronavirus (SCoV) 5′ UTR could be replaced by their counterparts from mouse hepatitis virus (MHV). However, the entire UTR could not be functionally substituted because of the location of the TRS (Kang et al., 2006). The current study is the first to show that the type 1 5′ UTR can have a regulatory function in the type 2 genomic backbone and remain fully functional. The chimeric virus vTLV8 displayed similar virologic characteristics to the WT, which implies that the substantial differences in biological properties between type 1 and type 2 PRRSV may not be due to the 5′ UTR. In addition, we performed related research to explore the origin of the 5′ UTR 5′ terminal exogenous sequences, and the results showed that the insertion sequence which was used for repair was template independent (Gao et al., 2012). We found that SL1 and SL2 of the PRRSV 5′ UTR were important cis-acting elements in viral replication and infectivity (Gao et al., 2012; Lu et al., 2011). This study suggests that LTH, especially the top loop in which the TRS located is another cis-acing element in the life cycle of PRRSV. Taken together, the results of this study are consistent with the conclusion of our previous work (Gao et al., 2012; Lu et al., 2011). The secondary structure elements rather than the authentic 5′-proximal primary sequence, are probably indispensable for PRRSV infectivity. This study provides a useful platform for further study on the structural and functional analysis of the PRRSV 5′ UTR.

References

Alexander, O., Pasternak, W.J.M.S.a.E.J.S., 2006. Nidovirus transcription: how to make sense…? J. Gen. Virol. 87, 1403–1421.

Alvarez, D.E., Lodeiro, M.F., Luduena, S.J., Pietrasanta, L.I., Gamarnik, A.V., 2005. Long-range RNA–RNA interactions circularize the dengue virus genome. J. Virol. 79 (11), 6631–6643.

Andino, R., Rieckhof, G.E., Baltimore, D., 1990. A functional ribonucleoprotein complex forms around the 5′ end of poliovirus RNA. Cell 63 (2), 369–380.

Barton, D.J., O'Donnell, B.J., Flanegan, J.B., 2001. 5′ cloverleaf in poliovirus RNA is a cis-acting replication element required for negative-strand synthesis. EMBO J. 20 (6), 1439–1448.

Born, E.V.D., Gultyaev, A.P., Snijder, E.J., 2004. Secondary structure and function of the 5′-proximal region of the equine arteritis virus RNA genome. RNA 10 (3), 424–437.

Born, E. v. d., Posthuma, C.C., Gultyaev, A.P., Snijder, E.J., 2005. Discontinuous subgenomic RNA synthesis in arteriviruses is guided by an RNA hairpin structure located in the genomic leader region. J. Virol. 79 (10), 6312–6324.

Cavanagh, D., 1997. Nidovirales: a new order comprising Coronaviridae and Arteriviridae. Arch. Virol. 142 (3), 629–633.

De Rijk, P., Wuyts, J., De Wachter, R., 2003. RnaViz 2: an improved representation of RNA secondary structure. Bioinformatics 19 (2), 299–300.

Dumas, E., Staedel, C., Colombat, M., Reigadas, S., Chabas, S., Astier-Gin, T., Cahour, A., Litvak, S., Ventura, M., 2003. A promoter activity is present in the DNA sequence corresponding to the hepatitis C virus 5′ UTR. Nucleic Acids Res. 31 (4), 1275–1281.

Fang, Y., Snijder, E.J., 2010. The PRRSV replicase: exploring the multifunctionality of an intriguing set of nonstructural proteins. Virus Res. 154 (1–2), 61–76.

Filomatori, C.V., Lodeiro, M.F., Alvarez, D.E., Samsa, M.M., Pietrasanta, L., Gamarnik, A.V., 2006. A 5′ RNA element promotes dengue virus RNA synthesis on a circular genome. Genes Dev. 20 (16), 2238–2249.

Filomatori, C.V., Lodeiro, M.F., Alvarez, D.E., Samsa, M.M., Pietrasanta, L., Gamarnik, A.V., 2007. A 5′ RNA element promotes dengue virus RNA synthesis on a circular genome. Genes Dev. 20, 2238–2249.

Forsberg, R., 2005. Divergence time of porcine reproductive and respiratory syndrome virus subtypes. Mol. Biol. Evol. 22, 2131–2134.

Frolov, I., Hardy, R., Rice, C.M., 2001. Cis-acting RNA elements at the 5′ end of Sindbis virus genome RNA regulate minus- and plus-strand RNA synthesis. RNA 7 (11), 1638–1651.

Frolov, I., McBride, M.S., Rice, C.M., 1998. Cis-acting RNA elements required for replication of bovine viral diarrhea virus-hepatitis C virus 5′ nontranslated region chimeras. RNA 4 (11), 1418–1435.

Gallie, D.R., 1998. A tale of two termini: a functional interaction between the termini of an mRNA is a prerequisite for efficient translation initiation. Gene 216 (1), 1–11.

Gamarnik, A.V., Andino, R., 1998. Switch from translation to RNA replication in a positive-stranded RNA virus. Genes Dev. 12 (15), 2293–2304.

Gao, F., Lu, J., Yao, H., Wei, Z., Yang, Q., Yuan, S., 2012. Cis-acting structural element in 5′ UTR is essential for infectivity of porcine reproductive and respiratory syndrome virus. Virus Res. 163 (1), 108–119.

Halbur, P.G., Paul, P.S., Frey, M.L., Landgraf, J., Eernisse, K., Meng, X.J., Lum, M.A., Andrews, J.J., Rathje, J.A., 1995. Comparison of the pathogenicity of two US porcine reproductive and respiratory syndrome virus isolates with that of the Lelystad virus. Vet. Pathol. 32 (6), 648–660.

Hanada, K., Suzuki, Y., Nakane, T., Hirose, O., Gojobori, T., 2005. The origin and evolution of porcine reproductive and respiratory syndrome viruses. Mol. Biol. Evol. 22 (4), 1024–1031.

Herold, J., Andino, R., 2000. Poliovirus requires a precise 5′ end for efficient positive-strand RNA synthesis. J. Virol. 74 (14), 6394–6400.

Kang, H., Feng, M., Schroeder, M.E., Giedroc, D.P., Leibowitz, J.L., 2006. Putative cis-acting stem-loops in the 5′ untranslated region of the severe acute respiratory syndrome coronavirus can substitute for their mouse hepatitis virus counterparts. J. Virol. 80 (21), 10600–10614.

Khromykh, A.A., Kondratieva, N., Sgro, J.Y., Palmenberg, A., Westaway, E.G., 2003. Significance in replication of the terminal nucleotides of the flavivirus genome. J. Virol. 77 (19), 10623–10629.

Liao, H.X., Chen, X., Munshaw, S., Zhang, R., Marshall, D.J., Vandergrift, N., Whitesides, J.F., Lu, X., Yu, J.S., Hwang, K.K., Gao, F., Markowitz, M., Heath, S.L., Bar, K.J., Goepfert, P.A., Montefiori, D.C., Shaw, G.C., Alam, S.M., Margolis, D.M., Denny, T.N., Boyd, S.D., Marshal, E., Egholm, M., Simen, B.B., Hanczaruk, B., Fire, A.Z., Voss, G., Kelsoe, G., Tomaras, G.D., Moody, M.A., Kepler, T.B., Haynes, B.F., 2011. Initial antibodies binding to HIV-1 gp41 in acutely infected subjects are polyreactive and highly mutated. J. Exp. Med. 208 (11), 2237–2249.

Liu, Y., Wimmer, E., Paul, A.V., 2009. Cis-acting RNA elements in human and animal plus-strand RNA viruses. Biochim. Biophys. Acta 1789 (9–10), 495–517.

Lodeiro, M.F., Filomatori, C.V., Gamarnik, A.V., 2009. Structural and functional studies of the promoter element for dengue virus RNA replication. J. Virol. 83 (2), 993–1008.

Lu, J., Gao, F., Wei, Z., Liu, P., Liu, C., Zheng, H., Li, Y., Lin, T., Yuan, S., 2011. A 5′-proximal stem-loop structure of 5′ untranslated region of porcine reproductive and respiratory syndrome virus genome is key for virus replication. Virol. J. 8, 172.

Matanin, B.M., Huang, Y., Meng, X.J., Zhang, C., 2008. Purification of the major envelop protein GP5 of porcine reproductive and respiratory syndrome virus (PRRSV) from native virions. J. Virol. Methods 147 (1), 127–135.

Meng, X.J., Paul, P.S., Halbur, P.G., 1994. Molecular cloning and nucleotide sequencing of the 3′-terminal genomic RNA of the porcine reproductive and respiratory syndrome virus. J. Gen. Virol. 75 (Pt 7), 1795–1801.

Meulenberg, J.J., de Meijer, E.J., Moormann, R.J., 1993a. Subgenomic RNAs of Lelystad virus contain a conserved leader–body junction sequence. J. Gen. Virol. 74 (Pt 8), 1697–1701.

Meulenberg, J.J., Hulst, M.M., de Meijer, E.J., Moonen, P.L., den Besten, A., de Kluyver, E.P., Wensvoort, G., Moormann, R.J., 1993b. Lelystad virus, the causative agent of porcine epidemic abortion and respiratory syndrome (PEARS), is related to LDV and EAV. Virology 192 (1), 62–72.

Mihalek, R.M., Banerjee, P.K., Korpi, E.R., Quinlan, J.J., Firestone, L.L., Mi, Z.P., Lagenaur, C., Tretter, V., Sieghart, W., Anagnostaras, S.G., Sage, J.R., Fanselow, M.S., Guidotti, A., Spigelman, I., Li, Z., DeLorey, T.M., Olsen, R.W., Homanics, G.E., 1999. Attenuated sensitivity to neuroactive steroids in gamma-aminobutyrate type A receptor delta subunit knockout mice. Proc. Nat. Acad. Sci. U.S.A. 96 (22), 12905–12910.

Murtaugh, M.P., Elam, M.R., Kakach, L.T., 1995. Comparison of the structural protein coding sequences of the VR-2332 and Lelystad virus strains of the PRRS virus. Arch. Virol. 140 (8), 1451–1460.

Nagashima, S., Sasaki, J., Taniguchi, K., 2005a. The 5′-terminal region of the Aichi virus genome encodes cis-acting replication elements required for positive- and negative-strand RNA synthesis. J. Virol. 79 (11), 6918–6931.

Nagashima, S., Sasaki, J., Taniguchi, K., 2005b. The 5′-terminal region of the aichi virus genome encodes cis-acting replication elements required for positiveand negative-strand RNA synthesis. J. Virol. 79 (11), 6918–6931.

Nelsen, C.J., Murtaugh, M.P., Faaberg, K.S., 1999. Porcine reproductive and respiratory syndrome virus comparison: divergent evolution on two continents. J. Virol. 73 (1), 270–280.

Oleksiewicz, M.B., Botner, A., Nielsen, J., Storgaard, T., 1999. Determination of 5′-leader sequences from radically disparate strains of porcine reproductive and respiratory syndrome virus reveals the presence of highly conserved sequence motifs. Arch. Virol. 144 (5), 981–987.

Pasternak, A.O., Spaan, W.J., Snijder, E.J., 2006. Nidovirus transcription: how to make sense…? J. Gen. Virol. 87 (Pt 6), 1403–1421.

Rijnbrand, R., Abell, G., Lemon, S.M., 2000. Mutational analysis of the GB virus B internal ribosome entry site. J. Virol. 74 (2), 773–783.

Rijnbrand, R., van der Straaten, T., van Rijn, P.A., Spaan, W.J., Bredenbeek, P.J., 1997. Internal entry of ribosomes is directed by the 5′ noncoding region of classical swine fever virus and is dependent on the presence of an RNA pseudoknot upstream of the initiation codon. J. Virol. 71 (1), 451–457.

Sawicki, S.G., Sawicki, D.L., 1995. Coronaviruses use discontinuous extension for synthesis of subgenome-length negative strands. Adv. Exp. Med. Biol. 380, 499–506.

Snijder, E.J., 2001. Arterivirus RNA synthesis dissected. Nucleotides, membranes, amino acids, and a bit of zinc. Adv. Exp. Med. Biol. 494, 241–253.

Snijder, E.J., Meulenberg, J.J., 1998. The molecular biology of arteriviruses. J. Gen. Virol. 79 (Pt 5), 961–979.

Sun, Z., Liu, C., Tan, F., Gao, F., Liu, P., Qin, A., Yuan, S., 2010. Identification of dispensable nucleotide sequence in 3′ untranslated region of porcine reproductive and respiratory syndrome virus. Virus Res. 154 (1–2), 38–47.

Sun, Z., Wang, J.Y., Zhang, J.W., Qin, A.J., Yuan, S.S., 2007. Identification of porcine reproductive and respiratory syndrome virus regulation sequence in 3′-untranslated region. Wei Sheng Wu Xue Bao 47 (5), 774–778.

TR, F., B, M., 1989. Structure and stability of mRNA synthesized by vaccinia virus-encoded bacteriophage T7 RNA polymerase in mammalian cells. Importance of the 5′ untranslated leader. J. Mol. Biol. 206 (2), 333–348.

Van Den Born, E., Gultyaev, A.P., Snijder, E.J., 2004. Secondary structure and function of the 5′-proximal region of the equine arteritis virus RNA genome. RNA 10 (3), 424–437.

van Marle, G., Dobbe, J.C., Gultyaev, A.P., Luytjes, W., Spaan, W.J., Snijder, E.J., 1999. Arterivirus discontinuous mRNA transcription is guided by base pairing between sense and antisense transcription-regulating sequences. Proc. Nat. Acad. Sci. U.S.A. 96 (21), 12056–12061.

Wang, Y., Liang, Y., Han, J., Burkhart, K.M., Vaughn, E.M., Roof, M.B., Faaberg, K.S., 2008. Attenuation of porcine reproductive and respiratory syndrome virus strain MN184 using chimeric construction with vaccine sequence. Virology 371 (2), 418–429.

Warter, L., Cohen, L., Benureau, Y., Chavez, D., Yang, Y., Bodola, F., Lemon, S.M., Traboni, C., Lanford, R.E., Martin, A., 2009. A cooperative interaction between nontranslated RNA sequences and NS5A protein promotes in vivo fitness of a chimeric hepatitis C/GB virus B. PLoS One 4 (2), e4419.

Yu, D., Lv, J., Sun, Z., Zheng, H., Lu, J., Yuan, S., 2009. Reverse genetic manipulation of the overlapping coding regions for structural proteins of the type II porcine reproductive and respiratory syndrome virus. Virology 383 (1), 22–31.

Yuan, S., Mickelson, D., Murtaugh, M.P., Faaberg, K.S., 2001. Complete genome comparison of porcine reproductive and respiratory syndrome virus parental and attenuated strains. Virus Res. 79 (1–2), 189–200.

Yuan, S., Wei, Z., 2008. Construction of infectious cDNA clones of PRRSV: separation of coding regions for nonstructural and structural proteins. Sci. China, Ser. C Life Sci. 51 (3), 271–279.

Zheng, H., Sun, Z., Zhu, X.Q., Long, J., Lu, J., Lv, J., Yuan, S., 2010. Recombinant PRRSV expressing porcine circovirus sequence reveals novel aspect of transcriptional control of porcine arterivirus. Virus Res. 148 (1-2), 8–16.

Zuker, M., 2003. Mfold web server for nucleic acid folding and hybridization prediction. Nucleic Acids Res. 31 (13), 3406–3415.